Supplementary Information for:

Photophysical Characterization and Time-Resolved Spectroscopy of a Anthradithiophene Dimer: Exploring the Role of Conformation in Singlet Fission

Jacob C. Dean,[1] Ruomeng Zhang,[1] Rawad K. Hallani,[2,4] Ryan D. Pensack,[1] Samuel N. Sanders,[3] Daniel G. Oblinsky,[1] Sean R. Parkin,[2] Luis M. Campos,[3] John E. Anthony,[2] and Gregory D. Scholes[1*]

[1] *Department of Chemistry, Princeton University, Princeton, NJ 08544*
[2] *Department of Chemistry, University of Kentucky, Lexington, KY 40506*
[3] *Department of Chemistry, Columbia University, New York, NY 10027*
[4] Current address: *KAUST Solar Centre, King Abdullah University of Science and Technology, Thuwal, Saudi Arabia*

1. Synthesis and characterization of 2ADT

In a flame dried round bottom flask equipped with a stir bar, mono-silylated TIBS ADT (ref 40) (200mg, 0.340 mmol) was dissolved in 15 ml of dry THF. At room temperature, LiHMDS was added (0.340ml, 1M solution in Hexane, 0.340 mmol), and 1,2-Bis(chlorodimethylsilyl)ethane (39 mg, 0.170mmol) to the solution and the reaction was stirred at room temperature. After 1 hour, the reaction was quenched with water and extracted with ethyl acetate. The solution was dried using $MgSO_4$, filtered, and concentrated. The crude product was purified using chromatography in 95:5 (hexane: DCM) eluent. The pure product was recrystallized in acetone to produce 60% red crystals. MP 198 °C. MS (MALDI, DHB matrix) m/z 1287 $(M-CH_3)^+$. ^1H NMR (400MHz, CDCl3): δ 9.31 (m, 4H), 9.16 (m, 4H), 7.87 (m, 1H), 7.03 (m, 3H), 2.75 (m, 6H), 1.79 (m, 40H), 1.56 (m, 12H), 1.13 (m, 12H) ppm. ^{13}C-NMR (100 MHz, CDCl3): δ 184.3, 182.5, 167.2, 164.2, 157.8, 154.1, 142.1, 136.5, 136.4, 133.6, 129.9, 129.2, 124.9, 120.4, 120.3, 120.2, 117.1, 116.7, 108.4, 103.6, 102.9, 102.6, 102.9, 26.8, 25.6, 25.5, 9.6 ppm.

2. Steady-state spectroscopy and time-resolved fluorescence of 2ADT in various solvents

Absorption and fluorescence spectra of 2ADT were taken in a variety of solvents and the results are shown in Figure S1. The spectra are arranged in order of solvent polarity index, and for cyclohexane, toluene, dichloromethane, and acetone (excluding THF solvents) there appears to be a trend in polarity and excimer emission intensity ($\lambda > 600$ nm). As discussed in the main text, the relative fluorescence intensity in that region is predominantly dictated by the total lifetime of the excimer intermediate. Therefore the intensity is larger for larger formation rates and smaller internal conversion rates, both of which are more optimal in acetone versus toluene. This interpretation is evidenced through comparison with TRF measurements of 2ADT in the variety of solvents given in Figure S1, which indicate a trend in relative excimer emission intensity with its rate of formation (taken from fitting the fluorescence decay with a biexponential fit). Those results are given in Table S1, and τ_1 is associated with the time constant for formation of the excimer exciton in the *cis* conformer, whereas τ_2 is associated with radiative decay of the minor *trans* conformer. Indeed, for all of the solvents studied in this work, the relative emission intensity of the excimer state correlates with its formation rate even for THF solvents which yield noticeably longer formation times compared to the other polar solvents studied. Figure S2 shows the rate of excimer exciton formation plotted against the solvent polarity and refractive

index again indicating some correlation with solvent polarity excluding THF, but no clear correlation with refractive index.
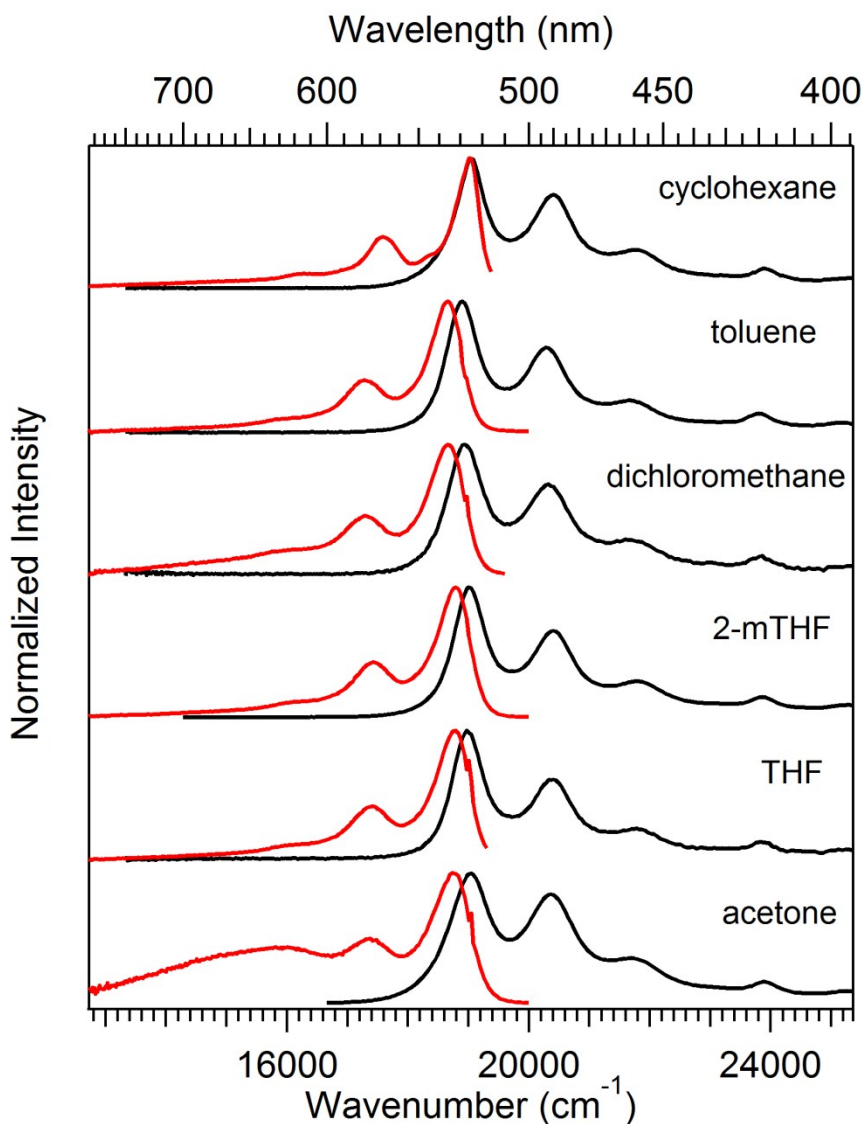
Figure S1. Absorption (black) and fluorescence (red) spectra of 2ADT in cyclohexane, toluene, dichloromethane, 2-methylTHF, THF, and acetone solvents. All fluorescence spectra are corrected and were acquired with an excitation wavelength at the peak of the absorption spectrum.
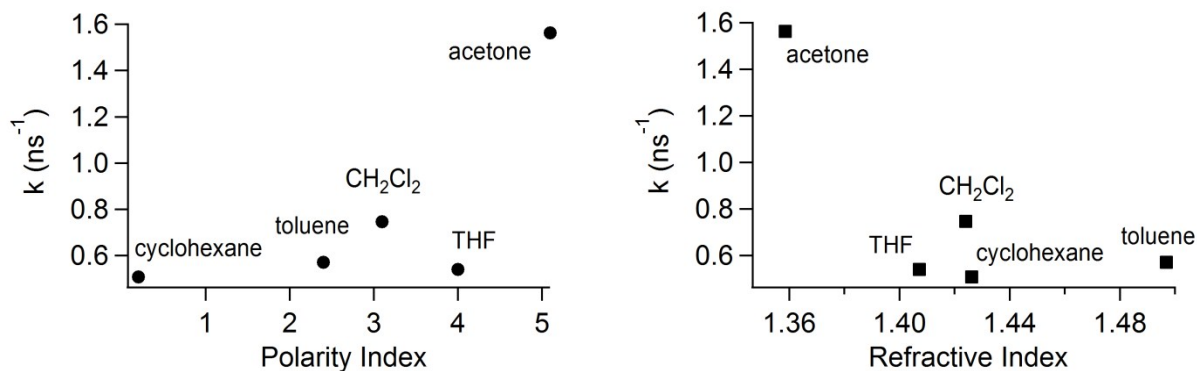
Figure S2. Comparison of the excimer exciton formation rate taken from TRF measurements to the solvent (left) polarity and (right) refractive index.

Table S1. Time constants for fluorescence decay from biexponential time-resolved fluorescence fitting of 2ADT in various solvents. Values in parentheses indicate relative amplitudes of each component.

Solvent	τ_1 (ns)	τ_2 (ns)
Cyclohexane	1.97 ± 0.01 (0.85)	8.48 ± 0.20 (0.15)
Toluene	1.75 ± 0.01 (0.93)	8.20 ± 0.51 (0.07)
Dichloromethane	1.34 ± 0.00 (0.88)	9.67 ± 0.10 (0.12)
THF	1.85 ± 0.01 (0.93)	7.79 ± 0.33 (0.07)
Acetone	0.64 ± 0.00 (0.68)	9.59 ± 0.13 (0.32)

As discussed in the main text there is a clear solvent-dependency on the excimer rate, presumed to be due mainly to a larger degree of pre-association on the ground state in polar solvents. We highlight that the apparent polarity dependence of the rate would also be consistent with charge-transfer (CT) state formation, in which the CT state is stabilized by polar solvents. However, the spectral evolution of the $S_1 \rightarrow S_n$ ESA features in TA is more consistent with excimer exciton formation, which results in a similar blue-shifting of all bands as the population moves away from the Franck-Condon region. The apparent stabilization of the excimer geometry by polar solvents however would imply enhanced CT-character of the excimer state generally, but such a scenario occurs via a virtual CT state still well above the locally-excited state and is never directly populated. Alternatively, the larger rate in polar solvents could be related to aggregation in solution leading to artificially faster rates due to inter-dimer interactions. However, we rule this possibility out on the basis of several observations:

(i) we would expect excimer formation in monomer solutions as well, and perhaps to a larger degree since those samples were typically run at about twice the concentration;

(ii) the rate for excimer exciton formation was concentration-independent over a concentration range varying about an order of magnitude;

(iii) dichloromethane is a polar solvent that readily dissolves both samples and exhibited the same trends in excimer formation.

## 3. Electronic transitions and molecular orbitals of ADT

The UV-visible absorption spectrum of ADT was analyzed in detail, and several features in the low-temperature absorption spectrum (Figure 3) were assignable to the first four electronic transitions in ADT with the aid of TDDFT predictions. TDDFT vertical excitation calculations yield not only the frequency and oscillator strength for electronic transitions, but also the transition dipole moment (TDM) direction and molecular orbitals involved in each transition. Those results are given in Figure S3, showing the molecular orbitals contributing the largest character to the electronic transition (largest coefficients) with the TDM direction given below each S_0–S_n label.
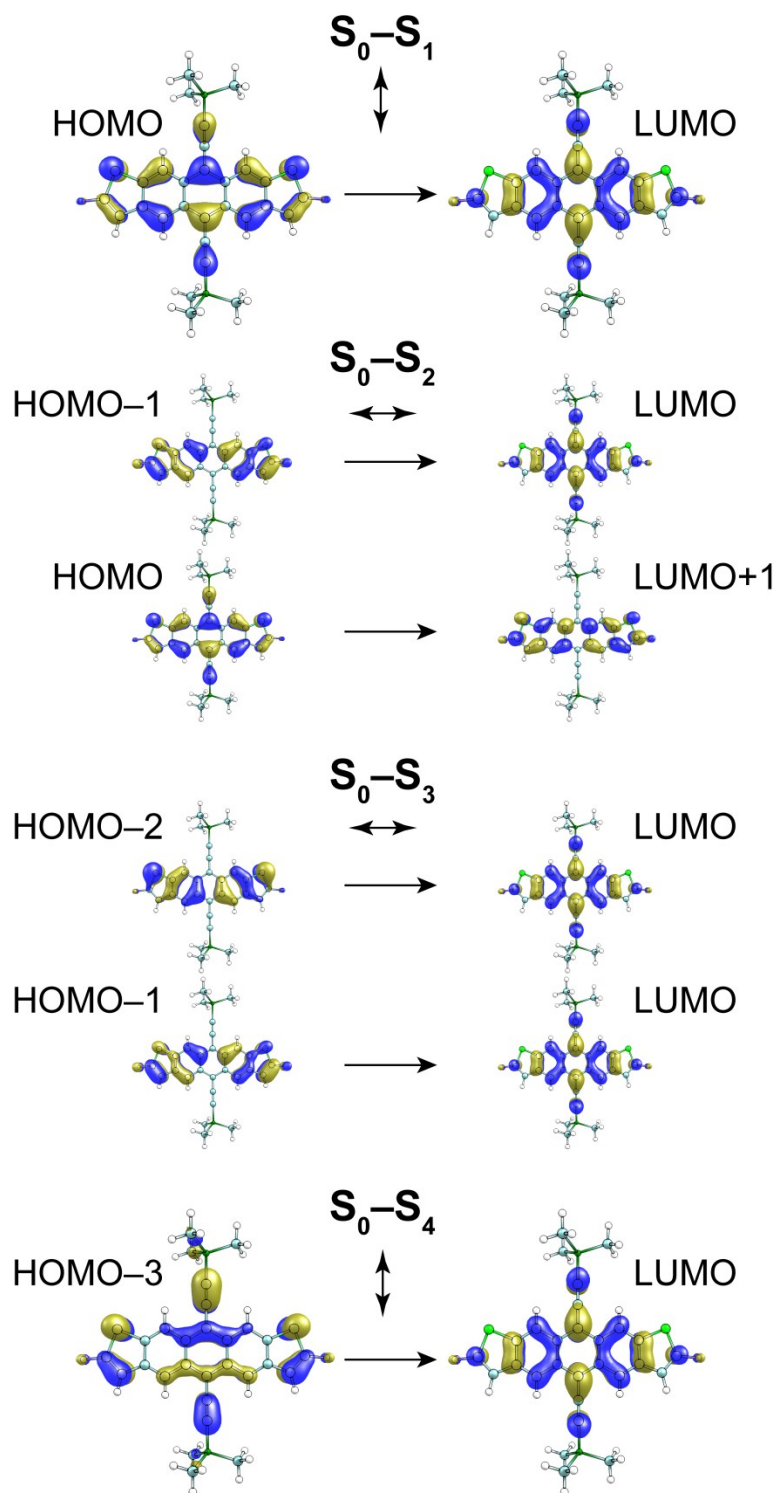
Figure S3. Molecular orbitals and transition dipole moment directions for the first four electronic transitions in ADT. The results were calculated at the TDDFT//CAM-B3LYP/6-31+G(d) level of theory.

4. Franck-Condon vibronic analysis of ADT

To explicitly characterize the vibronically-active modes in ADT/2ADT, a Franck-Condon simulation was undertaken using the DFT(TDDFT)//CAM-B3LYP/6-31+G(d) calculated ground and excited state geometries, along with their corresponding normal mode analyses. The simulation result is shown as red sticks in Figure S4 compared against the 77 K 2-mTHF spectrum. Remarkable agreement is found between experiment and theory, and the extended vibrational progressions can be directly assigned to sets of normal modes. The modes characterizing the ~730 and ~1475 cm^{-1} progressions are associated with in-plane ring modes of the ADT core, with the lower frequency set being associated with modes more delocalized over the whole five-ring core, and the higher frequency set appearing with larger amplitude and more localized to the anthracene center (example shown in Figure S4). Another mode carrying significant vibronic activity is a 226 cm^{-1} ADT core breathing mode (shown in the figure) appearing as an unresolved shoulder in the experimental spectrum. Figure S4 demonstrates the power of *ab initio* Franck-Condon simulations in assigning those vibrations activated under electronic excitation. Such predictions can be utilized to identify specific coordinates driving non-adiabatic dynamics or for characterizing the excited state potential energy surface.
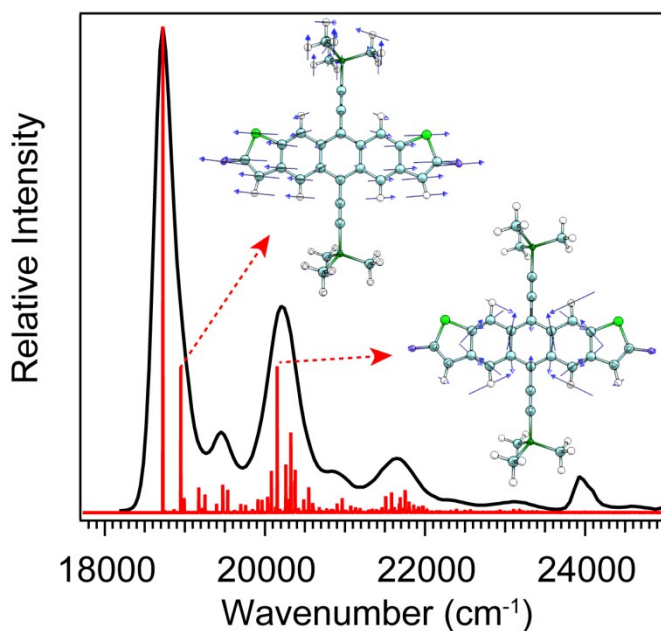

Figure S4. Zoomed S_0–S_1 region at 77 K with DFT Franck-Condon simulation shown as sticks for comparison. Two normal modes with extended progressions are shown.

5. Vibrational coherence in ADT

The occurrence of vibrational coherences in TA data was discussed briefly in the manuscript and shown in the inset of Figure 5 as an example. The generation of coherences in TA experiments requires sufficient bandwidth of the pump pulse to span all states involved in the coherence(s), usually the electronic origin transition and one vibrational quantum, as well as a pulse duration that is shorter than the vibrational coherence period. For the TA experiments reported here, the pulse duration is estimated to be ~70 fs based on prior diagnostics and the observed width of the coherent artifact in these measurements, suggesting a maximum coherence frequency resolution of ~475 cm^{-1}. Indeed, the predicted Franck-Condon active modes within this frequency window consists predominantly of the low-frequency ADT core breathing mode (Figure S4), and the vibrational coherence detected closely matches its frequency.

In order to isolate the coherent signals in the TA data, the population dynamics were subtracted from the data following a biexponential fit at each probe wavenumber. Figure S5a shows the TA data in toluene for the first 4 ps, and the right panel shows a zoomed portion where the quantum beats are most evident. The coherent TA data is shown in Figure S5b revealing clear oscillations in the GSB region, and a change in phase across the emission axis is clearly seen at ~18900 cm^{-1} as a node. This observation coupled with the absence of coherent oscillations in the S_1 ESA regions and SE region indicate that the coherence was generated predominantly on the ground state through impulsive Raman excitation.[1-4] Performing a fast Fourier Transform (FT) at each emission wavenumber yields the exact frequency of the coherence and its location in the TA map as shown in Figure S5c. The same analysis was done for ADT in acetone yielding analogous results, as shown in Figure S6. Interestingly the amplitude spans a larger region of the emission axis in accordance with the larger line-widths in acetone, revealing an additional node near 19300 cm^{-1}. Comparing with the raw TA data in Figure S6a, the second node is near a region of zero TA amplitude due to the overlapping GSB and ESA signals of opposite sign. Additionally though, some amplitude is found near 20000 cm^{-1} and below 19000 cm^{-1} at the strong $S_1 \rightarrow S_n$ band and SE bands respectively, indicating some excited state coherence. Figure S7 shows the trace taken at 19100 cm^{-1} and its Fourier transform for the toluene (black) and acetone (red) experiments for comparison. In both cases the FT yields a frequency of 240 cm^{-1}.
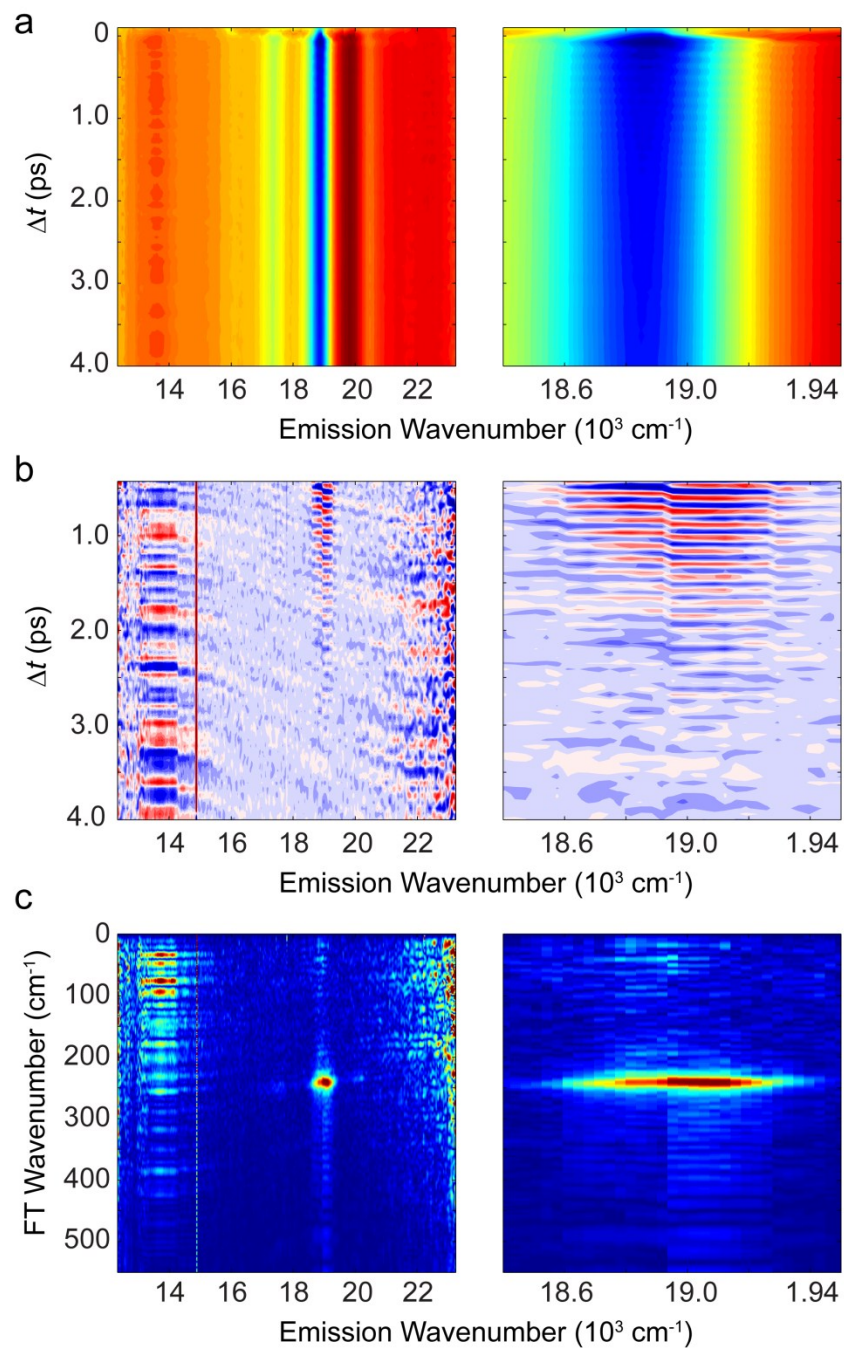
Figure S5. (a) TA map of ADT in toluene for first 4 ps in the visible (left) and GSB region (right). (b) Coherent TA and (c) Fourier transform map for ADT in toluene.
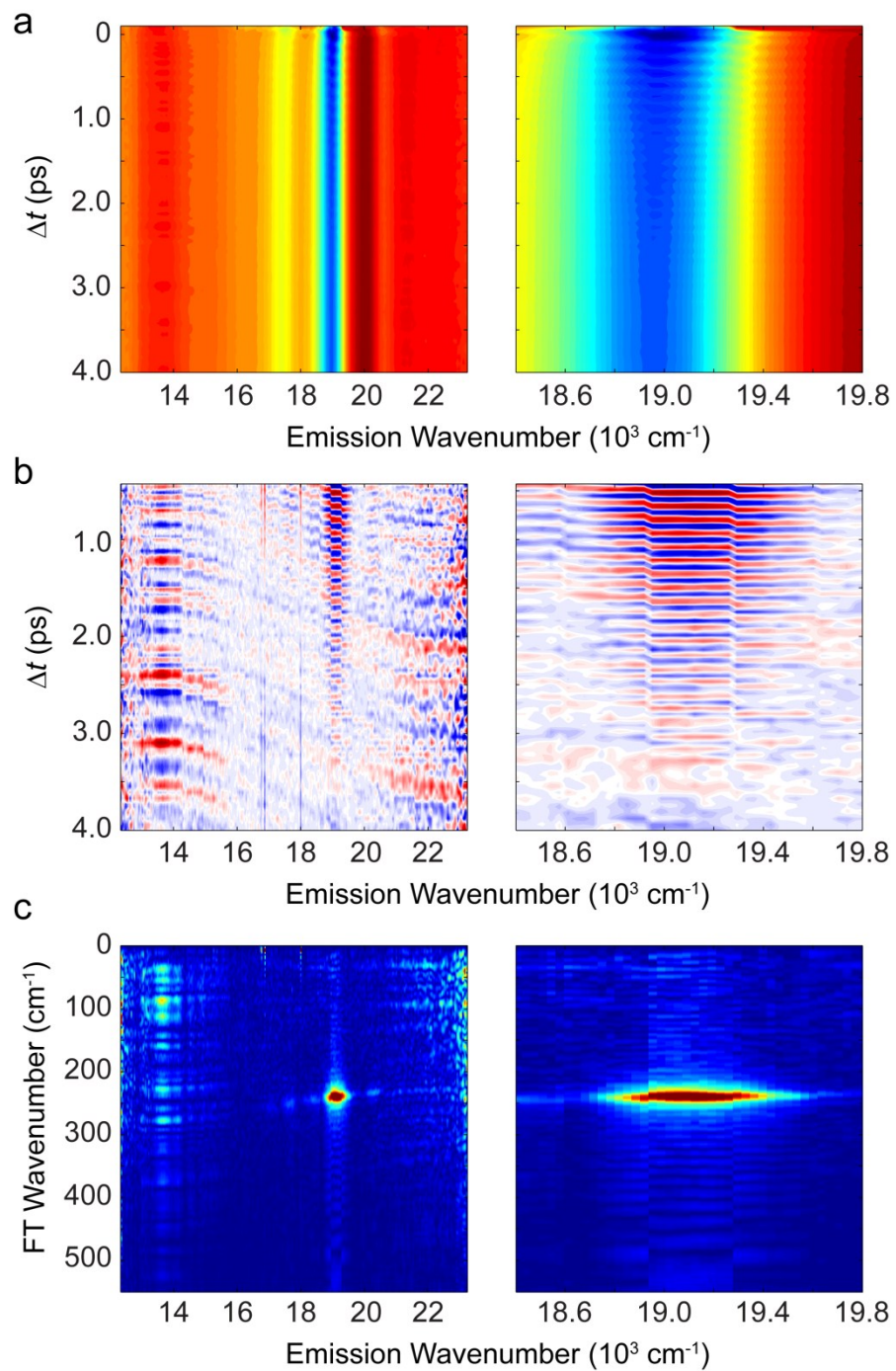
Figure S6. (a) TA map of ADT in acetone for first 4 ps in the visible (left) and GSB region (right). (b) Coherent TA and (c) Fourier transform map for ADT in acetone.
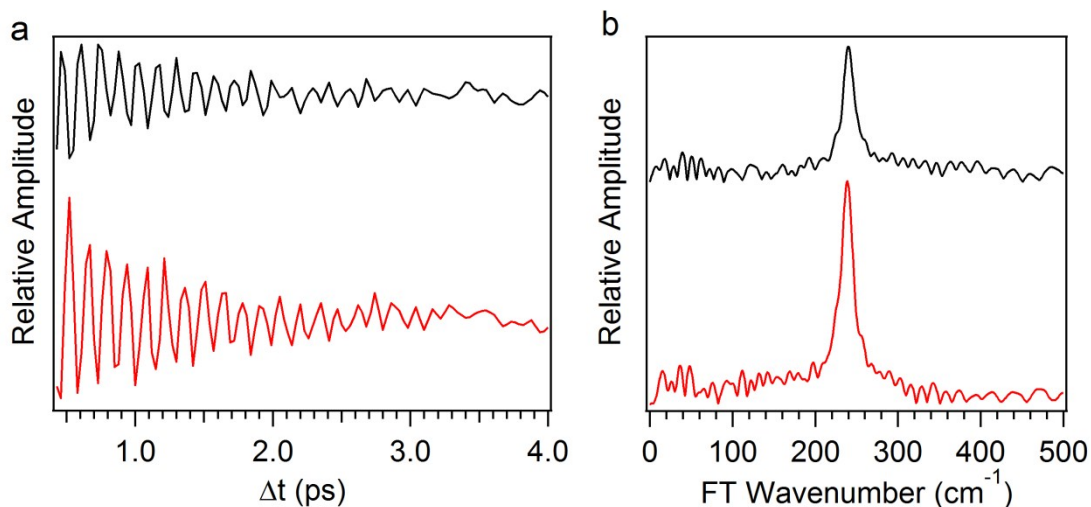
Figure S7. (a) Coherent traces of ADT taken at a probe wavenumber = 19100 cm^{-1} along with its corresponding (b) Fourier transform spectrum. Black indicates toluene solvent and red indicates acetone.

6. Isolating 2ADT conformer spectra in toluene and 2-mTHF solutions

The two low-energy conformers of 2ADT predicted through quantum chemical calculations were observed experimentally and assigned based on differences in TRF kinetics and a clear separation of excitation spectra in fluorescence spectroscopy. The latter was shown in Figure 9 for 2ADT in acetone where the red-shifted emission was observed at largest intensity. Analysis of those results indicated a minor *trans* conformer which appeared "monomer-like" in its excitation and fluorescence spectrum, and a *cis* conformer which yielded a red-shifted excitation spectrum akin to the respective absorption spectrum, along with a broadened red-shifted emission spectrum. While the isolation of steady-state spectra was easier to accomplish for acetone due to the stronger excimer contribution to the fluorescence spectrum and broader *cis* excitation features, the same was done for 2ADT in toluene and 2-mTHF and the results are summarized in Figure S8. The spectra are colored-coded/labeled similar to Figure 9, with the solid black traces designating the composite absorption spectrum, dashed traces indicating fluorescence excitation spectra taken while monitoring emission at the position marked by the respective dashed arrow, red traces are 2ADT fluorescence spectra from excitation at positions labeled by the corresponding arrows, and the blue traces are associated with ADT spectra for comparison.

The results for acetone are shown at the top of Figure S7 for reference. While the absorption spectrum of 2ADT in toluene differs from acetone slightly in the reduction of the red-shifted tail and a smaller relative intensity for the first vibronic band (both of which signify larger exciton coupling in acetone), two separable populations are still clearly borne out through fluorescence excitation spectroscopy. Again, the *trans* population is revealed through its near perfect overlap with the monomer absorption spectrum showing narrowed line-shapes and blue-shifted vibronic bands. For toluene and 2-mTHF, it was difficult to obtain a pure *cis* fluorescence spectrum due to the reduction in line-width of the *cis*-2ADT absorption band resulting in spectral overlap at the excitation wavelength. Nevertheless, the fluorescence spectra taken at the two excitation wavelengths clearly differ in the region between 13000–18000 cm^{-1} revealing the excimer signatures of the *cis* conformer.
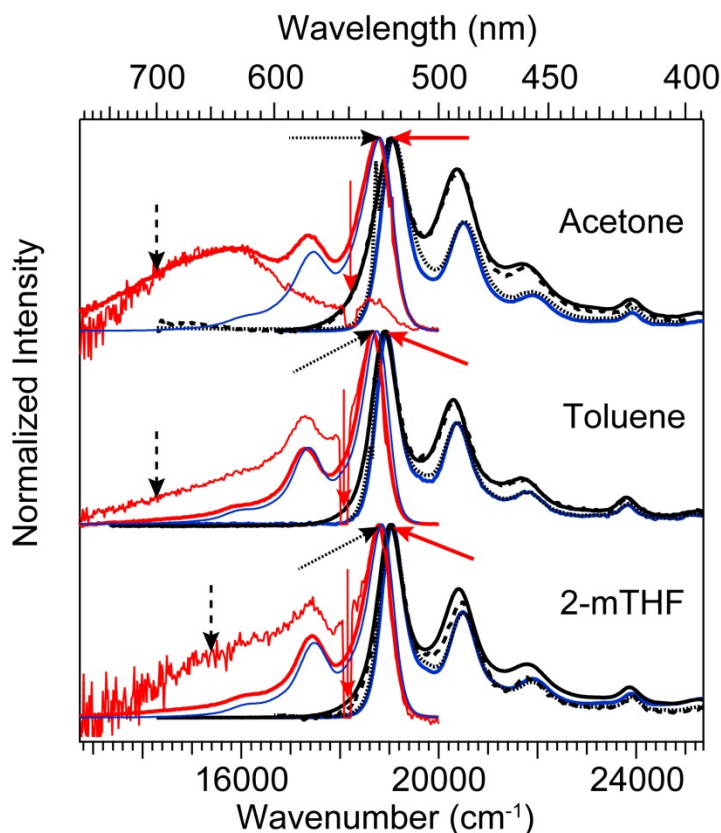
Figure S8. Separation of spectral contributions to absorption and fluorescence spectra of 2ADT. Solid black traces are absorption spectra, dashed black traces designate fluorescence excitation spectra taken while monitoring fluorescence at the position of the dashed arrows, red traces are fluorescence spectra acquired following excitation at the wavelength of the corresponding arrow, and blue traces are ADT spectra for reference.

References

1. S. D. McClure, D. B. Turner, P. C. Arpin, T. Mirkovic and G. D. Scholes, *J. Phys. Chem. B*, 2014, **118**, 1296-1308.
2. M. H. Vos, F. Rappaport, J. C. Lambry, J. Breton and J. L. Martin, *Nature*, 1993, **363**, 320-325.
3. J. A. Cina, P. A. Kovac, C. C. Jumper, J. C. Dean and G. D. Scholes, *J. Chem. Phys.*, 2016, **144**.
4. J. C. Dean, S. Rafiq, D. G. Oblinsky, E. Cassette, C. C. Jumper and G. D. Scholes, *J. Phys. Chem. A*, 2015, **119**, 9098-9108.